

# Crystallization kinetics of glass prepared with foundry slag

T. S. Leme<sup>1\*</sup>, R. S. Magalhães<sup>1</sup>, G. T. A. Santos<sup>1</sup>, S. R. Teixeira<sup>1</sup>, A. E. Souza<sup>1</sup>

<sup>1</sup>Universidade Estadual Paulista, Faculdade de Ciências e Tecnologia, Presidente Prudente, SP, Brazil

## Abstract

Iron foundry slag and hydrated lime were used in glass preparation by the melt-quenching method. The glass obtained was heat-treated using the thermal analysis technique. A crystallization kinetics study was carried out with glass powder samples using a non-isothermal method at five different heating rates by differential scanning calorimetry (DSC). Considering that few studies compare kinetic results obtained by different methods, in this work, the activation energy ( $E_a$ ) of the crystallization process was obtained using the Kissinger and Augis-Bennett models for comparison purposes. The  $E_a$  results showed negligible variation in comparing the methods used, nevertheless, linear fitting of crystallization peaks was slightly better by the Augis-Bennett than the Kissinger model. The Avrami index values showed an increasing nucleation rate for two stable phases and decreasing for the metastable phase present in the glass-ceramic. Avrami indexes obtained also indicated an interface-controlled particle growth, whose scanning electron microscopy images showed different morphologies of crystalline particles in the bulk of the glass matrix.

**Keywords:** slag, glass, glass-ceramic, crystallization, kinetics.

## INTRODUCTION

Production activities in any industrial process generate solid waste and undesirable by-products during the processing of raw materials [1]. The steel industry, in particular, encounters difficulties in handling its waste with different compositions and quantities, generated by the smelting process [2]. This waste is destined for a certified industrial landfill, which in turn is generally far from the region where the foundry is located. This waste handling is burdensome for the company, which often searches for alternatives that result in inappropriate waste disposal [2, 3]. Recycling is undoubtedly the most interesting alternative, from an economic or environmental point of view and often from a social aspect [4]. Foundry slag is one of the by-products generated in large quantities during the process. Its chemical composition may vary depending on the raw material used, the production process, and its storage [5]. Among its main constituents are simple oxides such as silicon oxide ( $\text{SiO}_2$ ), magnesium oxide ( $\text{MgO}$ ), iron oxide ( $\text{Fe}_2\text{O}_3$ ), and aluminum oxide ( $\text{Al}_2\text{O}_3$ ), which are present as major compounds [6]. Considering that silicon oxide is a glass-forming material, there are some works that have shown the transformation potential of silicate base residues into glass and glass-ceramic products of great usefulness. The process of obtaining glass-ceramic materials usually involves silicate (residue) vitrification, or a mixture of several residues, which begins with glass, followed by a crystallization process to obtain the glass-ceramic [7]. Teixeira et al. [8] obtained a glass-ceramic material of great importance in the civil industry, using sugar cane bagasse ashes as the main raw material. Folgueiras et al. [9] used discarded sand casting material as a partial substitute for silica to produce glass.

Other works show the use of a wide variety of casting slags for different applications, such as concrete aggregate [10, 11], non-plastic material embedded in structural red ceramic [12, 13], mortar additive [14], polymer composite reinforcement [15], and geopolymer bricks [16]. There are no studies in the literature on obtaining glass-ceramics from the slag from an iron casting foundry. Accordingly, the aim of this study was to determine the use of iron foundry slag for the production of glass and glass-ceramic materials.

There are methods described in the literature to evaluate the crystal nucleation and growth process in the glass matrix. These methods are generally called kinetic models [17, 18]. The kinetic process involves the crystallization of the glassy material, for which several model-fitting methods have been developed on the basis of phase change [19]. The study of isothermal kinetics is based on the mathematical model known as the Johnson-Mehl-Avrami-Kolmogorov (JMAK) model, developed in the period of 1937-1939 [7, 19]. Glass crystallization kinetics can be investigated isothermally or non-isothermally using thermal analysis techniques, such as differential scanning calorimetry (DSC) or differential thermal analysis (DTA). These methods have been shown to be appropriate for kinetic studies to obtain information about the nucleation and crystal growth mechanism [7, 19, 20]. Several models have been proposed to determine kinetic parameters for non-isothermal conditions, in which peak crystallization temperatures ( $T_p$ ) are determined from the thermal analysis curves [17]. Among these methods are the Kissinger and Augis-Bennett methods. Kissinger proposed a model that allows the determination of the crystallization activation energy ( $E_a$ ) according to [21-24]:

$$\ln\left(\frac{\beta}{T_p^2}\right) = -\frac{E_a}{R \cdot T_p} + \text{constant} \quad (\text{A})$$

where  $\beta$  is the heating rate,  $R$  is the universal gas constant,

\*thariany.sl@outlook.com

 <https://orcid.org/0000-0002-7933-9597>

and  $E_a$  is obtained by linear regression of  $\ln(\beta/T_p^2)$  versus  $1/T_p$ . The Augis-Bennett method provides the modified Kissinger method to determine the activation energy ( $E_a$ ) according to [25]:

$$\ln\left(\frac{\beta}{T_p - 300}\right) = -\frac{E_a}{R \cdot T_p} + \text{constant} \quad (\text{B})$$

where  $E_a$  is obtained by linear regression of the  $\ln[\beta/(T_p - 300)]$  versus  $1/T_p$ . The Avrami index ( $n$ ) is an important parameter for kinetics study since it provides information about crystal nucleation and growth [24-26]. With the  $E_a$  values obtained, the Avrami index ( $n$ ) can be calculated from Eq. C proposed by Augis-Bennett [25]:

$$n = \left(\frac{2.5}{\Delta T}\right) \cdot \frac{T^2}{\left(\frac{E_a}{R}\right)} \quad (\text{C})$$

where  $n$  is related to the predominant crystallization mechanism, and  $\Delta T$  corresponds to the width at half-height of the crystallization peak. In the present study, the Kissinger and Augis-Bennett models were used to determine the activation energy and the kinetic parameters of the glass-ceramic material obtained from the foundry slag. The kinetic values found by these methods were compared to evaluate their agreement.

## EXPERIMENTAL

The foundry slag used was collected at factories in Presidente Prudente county, São Paulo state, Brazil. The slag was ground and sieved using a 30 mesh sieve. An aliquot of slag was subjected to chemical analysis by X-ray fluorescence (XRF) spectroscopy using a Shimadzu EDX-7000 spectrometer to determine the chemical composition, in terms of oxide percentage. The quantitative analysis was done in the air using powdered material. The glass composition was determined using the XRF results of the slag and the ternary phase diagram system  $\text{SiO}_2$ - $\text{Al}_2\text{O}_3$ - $\text{CaO}$ . Slag was mixed with hydrated lime [ $\text{Ca}(\text{OH})_2$ ] and potassium carbonate ( $\text{K}_2\text{CO}_3$ ) to lower the melting point of silicon dioxide present in the slag. The glass melting temperature was determined using the method of Chengyu and Ying [27] and estimated to be below 1500 °C. The glass composition was 46 wt% slag, 40 wt% hydrated lime, and 14 wt% potassium carbonate.

The mixture was transferred to alumina crucibles (5 cm in diameter by 10 cm in height) and placed in an oven (1700 °C equipment, SF-M220605, Servifor) for melting using a heating rate of 20 °C/min up to 1450 °C

and a holding time of 1 h for melting of the components. Subsequently, the alumina crucible was removed from the oven and the liquid was quickly poured into a vessel containing distilled water for rapid cooling (melt-quenching method), producing a glass frit, which was milled down to particles of 80 µm. The glass powder was used to make pellets with 1 cm in diameter and 0.5 g mass, using a Shimadzu uniaxial manual press and 20 kN of force applied for 3 min. The pellet glass was thermally treated at 900 °C for 1.5 h with a heating rate of 10 °C/min using an EDG-2000 muffle to obtain the glass-ceramic. The glass and glass-ceramic were characterized by X-ray diffraction (XRD) using a Shimadzu XRD-6000 diffractometer, with  $\text{CuK}\alpha_1$  ( $\lambda=1.5406$  Å) and  $\text{CuK}\alpha_2$  ( $\lambda=1.5444$  Å) radiation, 40 kV voltage, and 30 mA current. Scanning was done in a  $2\theta$  range from 10° to 80°, using divergence and reception slits with 1° opening, in continuous mode, with 0.02° step and 2°/min scanning speed.

Glass crystallization kinetics was studied by the non-isothermal method, where a small amount of glass powder was subjected to thermal analysis, differential scanning calorimetry (DSC, SDT Q600, TA Instr.), from room temperature up to 1200 °C. DSC scanning was conducted under air flow (100 mL/min) using an alumina crucible as a reference at different heating rates (5, 10, 20, 25, and 30 °C/min). The crystallization activation energy was obtained from the equations proposed by the Kissinger and Augis-Bennett models. The Avrami index ( $n$ ) was determined with the modified Kissinger equation using the  $E_a$  values obtained by the Kissinger and Augis-Bennett models.

## RESULTS AND DISCUSSION

Table I shows the results of quantitative chemical analysis obtained from the XRF results of the foundry slag. The results showed that the main component, with the highest concentration in the slag, was  $\text{SiO}_2$  followed by  $\text{Fe}_2\text{O}_3$ ,  $\text{Al}_2\text{O}_3$ ,  $\text{MnO}$ ,  $\text{CaO}$ , and  $\text{MgO}$ . It is worth mentioning that, among the oxides determined,  $\text{SiO}_2$  was the oxide responsible for the glass network formation (network former). The higher or lower concentration of this oxide was directly related to the viscosity of the glassy material obtained. Alumina can act as a former or network modifier (as well as  $\text{Fe}_2\text{O}_3$ ,  $\text{ZrO}_2$ , and  $\text{TiO}_2$ ), being responsible for glass stability and also contributes to its viscosity. Calcium, magnesium, and potassium oxides act as network modifiers, contributing to the decrease in viscosity and melting point [28].

Fig. 1 shows the XRD patterns of the glass and glass-ceramic material obtained after glass heat-treatment at 900 °C for 1.5 h. The glass diffractogram (Fig. 1a)

Table I - Chemical composition (wt%) of slag by XRF analysis.

$\text{SiO}_2$	$\text{Fe}_2\text{O}_3$	$\text{Al}_2\text{O}_3$	$\text{MnO}$	$\text{CaO}$	$\text{MgO}$	$\text{TiO}_2$	$\text{Cr}_2\text{O}_3$	$\text{K}_2\text{O}$	$\text{ZrO}_2$
54.0	18.2	12.8	5.8	2.9	2.1	0.9	0.6	0.5	0.4

showed a band around  $2\theta=30^\circ$ , characteristic of amorphous material, indicating that the glass obtained had no structural ordering, as predicted. The diffractogram of the glass-ceramic material (Fig. 1b) showed the formation of three major crystalline phases: merwinite [ $\text{Ca}_3\text{Mg}(\text{SiO}_4)_2$ ], akermanite [ $\text{Ca}_2\text{Mg}(\text{Si}_2\text{O}_7)$ ], and calcium aluminum silicate ( $\text{CaAl}_2\text{SiO}_6$ ), identified by JPCDF files 89-2432, 35-592, and 31-249, respectively. It is worth remembering that some peaks, especially those with low intensity, corresponding to the calcium aluminum silicate phase, showed a slight displacement around their positions ( $2\theta$ ), suggesting that this phase may present small stoichiometric variations, resulting from complex reactions between metastable phases or even with a residual glass phase. These reactions are common in most glass-ceramics with multicomponent nature in their composition, as it is obtained with foundry slag [29].

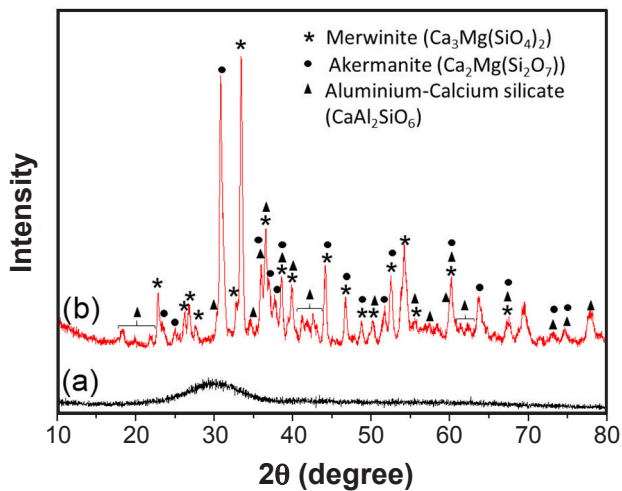


Figure 1: X-ray diffraction patterns of: a) glassy material; and b) glass-ceramic.

Fig. 2 shows the DSC thermogram and the peaks obtained for the different heating rates (5, 10, 20, 25, and 30 °C/min) up to 1200 °C. The results showed that with an increase in heating rate, the sample crystallization peaks around 900 °C were more evident. This was due to the higher energy per unit time provided by the system for phase crystallization. As this energy increased, the phase crystallization process occurred more rapidly and the heat flux was recorded more clearly.

Fig. 3 shows the crystallization peaks around 900 °C for different heating rates. It can be seen that the increase in heating rate influenced the peak position, shifting the crystallization temperature higher, as determined by the DSC curve. Crystallization peak fitting was performed to obtain a better definition of crystallization peak with temperature. The deconvolution of each peak was done, fitting three curves corresponding to the three major phases identified after crystallization. The peak fitting and deconvolution can be observed in Fig. 4. With the best fitting of the crystallization peaks, there was more than one peak in the heating rate of 10 and 25 °C/min. This might have

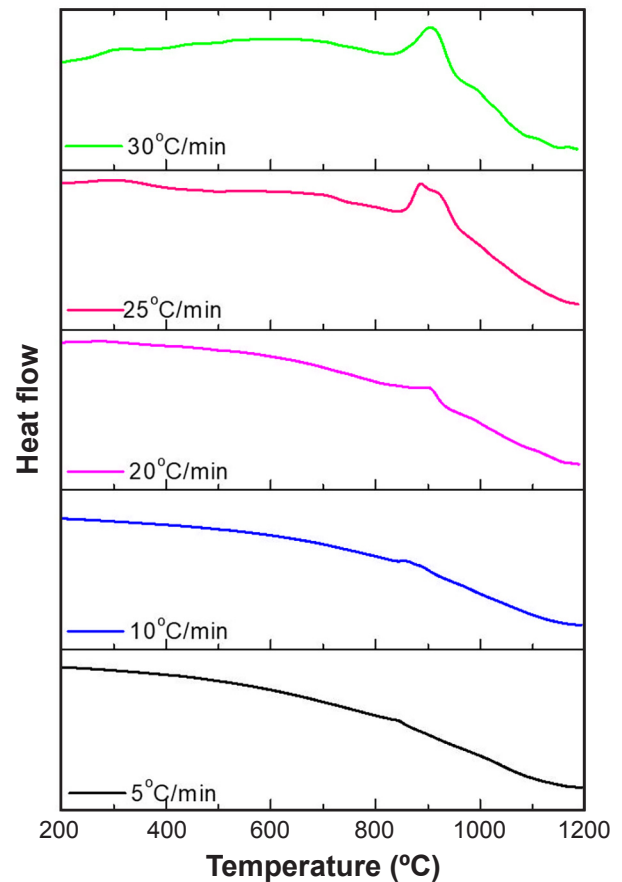


Figure 2: DSC thermograms of glassy samples for five different heating rates.

been associated with the presence of particles smaller than 80  $\mu\text{m}$  used in this work, which might have been selected at these two heating rates. According to Romero *et al.* [30], particles with different dimensions show variations in the crystallization and crystal growth processes. Fractions smaller than 100  $\mu\text{m}$  may exhibit crystallization peaks at slightly different temperatures, which increase with

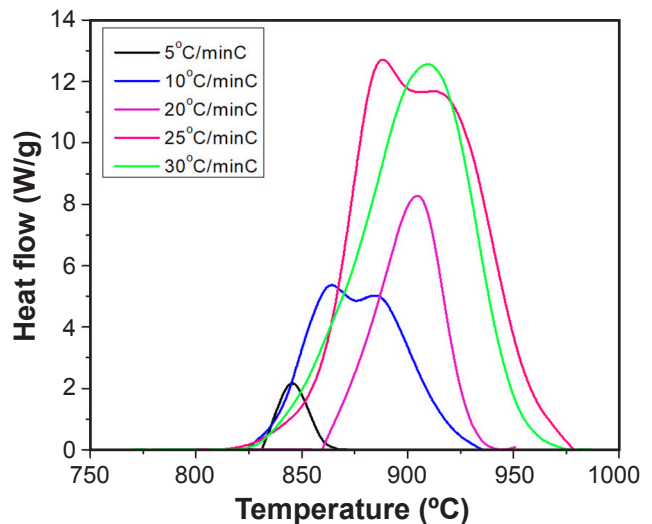


Figure 3: Crystallization peaks obtained for different heating rates.

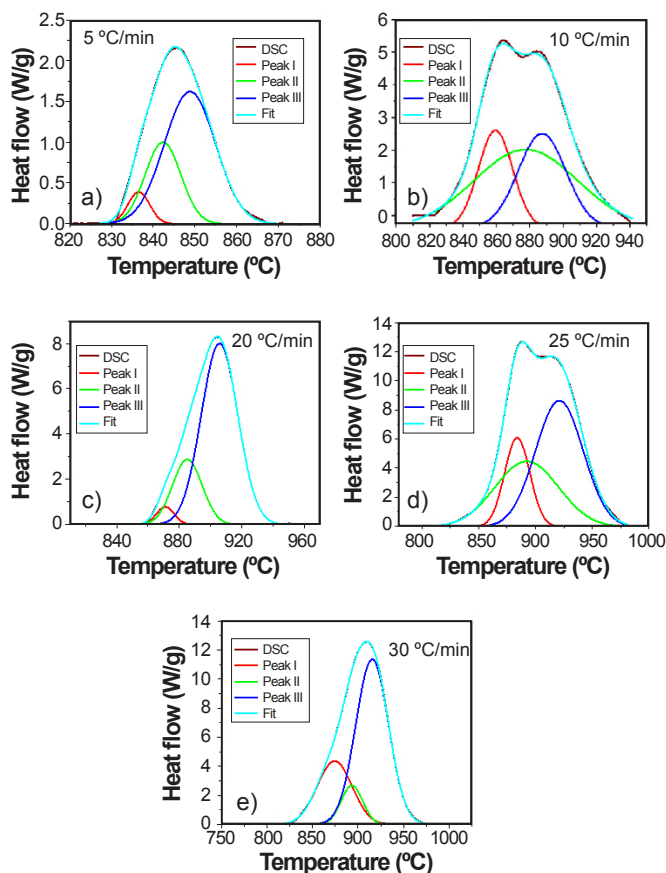


Figure 4: Deconvolution of crystallization peaks.

Table II - Peak temperatures (crystallization temperature -  $T_p$ , °C) for the DSC curves fitted for different heating rates.

Peak	Heating rate (°C/min)				
	5	10	20	25	30
I	836	859	872	883	895
II	842	876	888	893	905
III	848	887	905	921	925

decreasing particle size and heating rate [30]. By means of these fitting and deconvolution measures, the crystallization temperature ( $T_p$ ) for each peak according to the heating rate was obtained. The results are shown in Table II. Fitting showed that the crystallization temperature of peaks I, II, and III increased for their respective heating rate, indicating that the phases crystallized at slightly different temperatures.

For each adjusted peak, the activation energies were determined using the  $T_p$  shown in Table II. The activation energy was determined using the Kissinger and Augis-Bennett methods for comparison purposes. Fig. 5 shows  $\ln(\beta/T_p^2)$  plotted against  $1/T_p$  for the Kissinger equation and  $\ln[\beta/(T_p-300)]$  against  $1/T_p$  for the Augis-Bennett equation. Table III shows the activation energy ( $E_a$ ) values and the correlation coefficient ( $r$ ) of the three crystallization peaks obtained by the Kissinger and Augis-Bennet methods, calculated using the angular coefficient of the linear

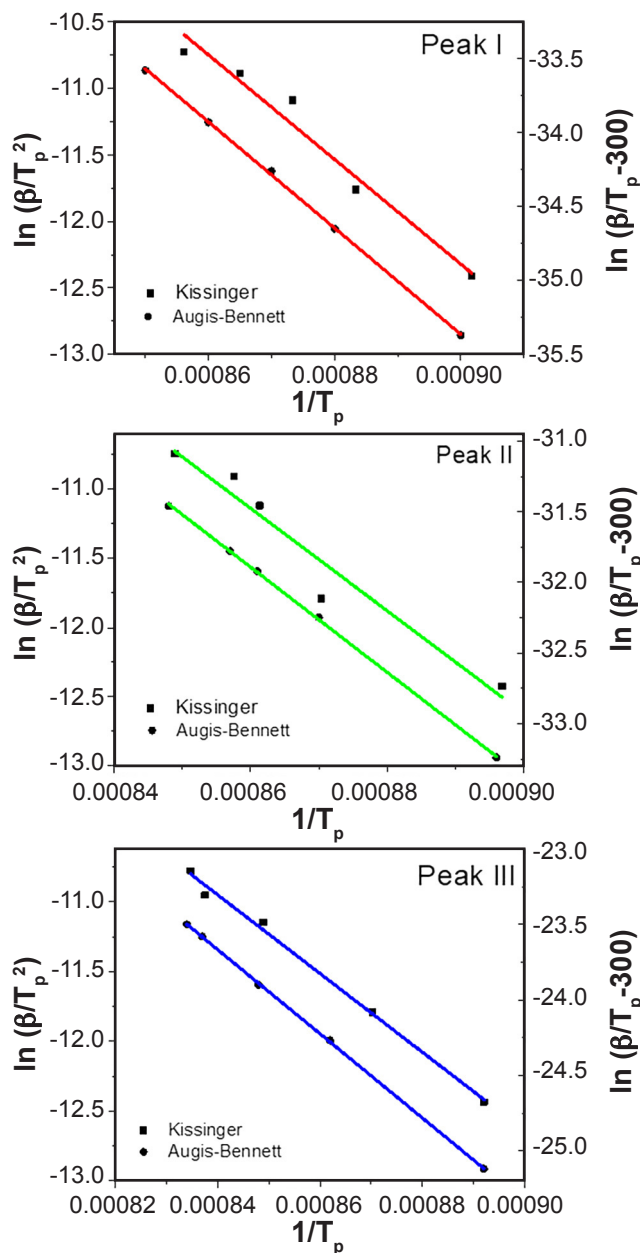


Figure 5: Kissinger and Augis-Bennett linear fitting.

Table III -  $E_a$  and  $r$  values obtained by different methods.

Peak	Kissinger		Augis-Bennett	
	$E_a$ (kJ/mol)	$r$	$E_a$ (kJ/mol)	$r$
I	326±34	0.984	298±4	0.999
II	308±43	0.972	309±3	0.999
III	234±9	0.997	232±2	0.999

regression fit, according to Eqs. A and B for each method. Calculations were performed according to the straight lines shown in Fig. 5.

It can be seen that  $E_a$  obtained with the Kissinger method for the three peaks showed a margin of error greater than that obtained with the Augis-Bennett method. However,

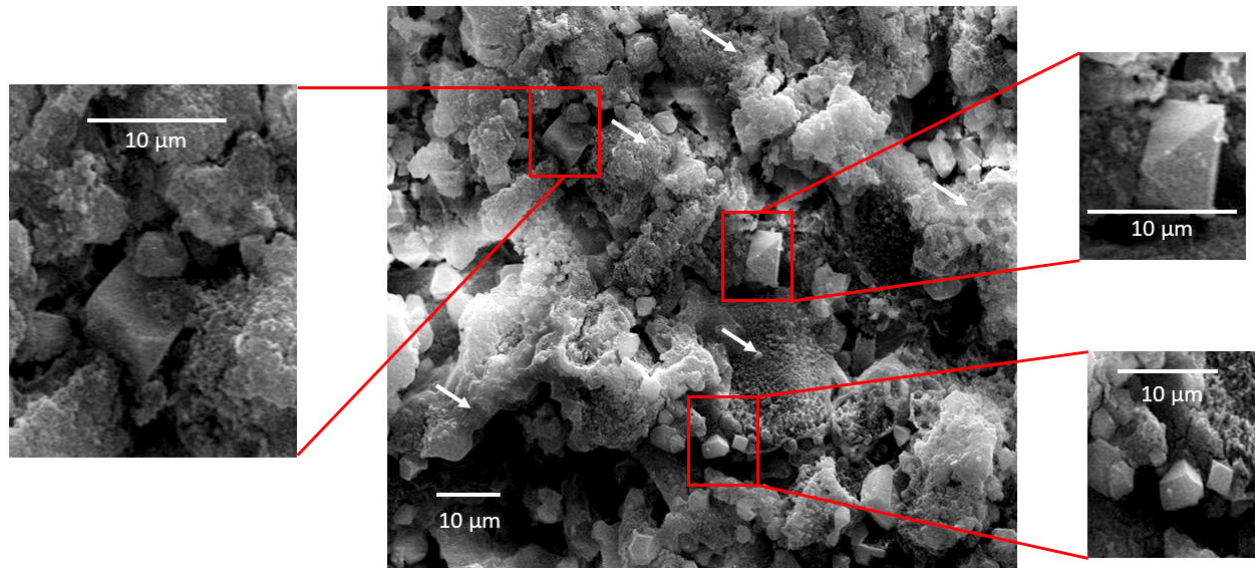


Figure 6: SEM images of the glass-ceramic sample treated at 900 °C for 1.5 h, after HF (0.5%) etching for 60 s. The arrows indicate the glassy region.

Table IV - Avrami index ( $n$ ) values using activation energy with the different methods.

Peak	$n$ (Kissinger $E_a$ )	$n$ (Augis-Bennett $E_a$ )
I	5.66	6.02
II	3.74	3.75
III	4.36	4.38

there was no significant difference between the two methods when comparing the  $E_a$  of each peak. The correlation coefficient of fit with the Augis-Bennett method was better than that obtained with the Kissinger method, being closer to 1. This explained a better linear fitting of the peaks, as observed in Fig. 5. In the literature, there are works on glass crystallization kinetics with similar compositions as ours and with crystallization temperatures close to or greater than that found in this work. Yu *et al.* [31], for example, studied the crystallization kinetics of glasses in the CaO-MgO-Al<sub>2</sub>O<sub>3</sub>-SiO<sub>2</sub> system containing different iron contents. The  $E_a$  values obtained ranged from 384 to 602 kJ/mol to the peaks with crystallization temperature between 990 and 1030 °C [31]. In the work of Teixeira *et al.* [32], whose crystallization kinetics was evaluated in glasses of the SiO<sub>2</sub>-Al<sub>2</sub>O<sub>3</sub>-CaO system,  $E_a$  in the order of 223 to 572 kJ/mol was found with crystallization peaks ranging from 879 to 1011 °C. It can be observed, therefore, that fluctuations in the  $E_a$  values corresponding to the crystallization peaks are directly related to the composition of the studied glasses, considering that different formed phases, coming from different glass compositions, require different energies to be formed.

The Avrami index ( $n$ ) was determined using the activation energy value of each peak, previously obtained by the Kissinger and Augis-Bennett methods. These indices were determined using Eq. C and the values are shown in Table IV. It can be seen that the Avrami indices for peaks

I and III were higher than 4, for both methods used. These values indicated an increasing nucleation rate [33-35]. The  $n$  value for peak II was between 3 and 4 indicating a decreasing nucleation rate [33-35]. From these results, we can assign peak II to the metastable phase (calcium silicate), which presents a decreasing nucleation rate when evolving to a stable phase. The I and III peaks corresponded to the akermanite and merwinite phases, respectively, whose increasing nucleation rates indicated the predominance in the glass-ceramic structure, as stable phases. According to Höland and Beall [29], akermanite presents itself as a minority phase in slag-based glass-ceramics, as it comes from elements that are not glass-forming. In this context, the akermanite can become less stable, when compared to the merwinite phase and, therefore, the activation energy for its nucleation and growth in relation to the merwinite phase is greater, as observed in Table III.

The scanning electron microscopy (SEM) images (Fig. 6) showed the presence of several particles with different morphologies crystallized inside the glassy region (indicated by arrows). This difference in morphology may be associated with the different crystalline phases present in the sample, although it was not possible to associate the morphologies to each phase. The Avrami indexes obtained indicated an interface-controlled growth of these observed particles.

## CONCLUSIONS

Glass and glass-ceramic material, composed of three crystalline phases, were successfully obtained from foundry slag. The kinetics around the single crystallization peak, deconvoluted into three other peaks corresponding to the crystallized phases, were studied by two different non-isothermal methods (Kissinger and Augis-Bennett). The results showed very close activation energy values for both methods, although the linear adjustment using the Augis-

Bennett method was slightly better. The Avrami index indicated for peaks I and III, corresponding to the stable phases akermanite and merwinite, respectively, an interface-controlled growth with an increasing nucleation rate. On the other hand, for peak II corresponding to the calcium silicate metastable phase, it indicated an interface-controlled growth with decreasing nucleation rate. SEM images of the material showed three-dimensional crystal growth with polyhedron morphology. The kinetic parameters evaluated by the different methods used showed good approximations, suggesting that the methods converge the kinetics studies for similar results. In addition, they revealed important characteristics of the nucleation and growth of crystals formed in a glassy matrix obtained from foundry industry residues.

## ACKNOWLEDGMENTS

To MPE, MPF (025/2011-0404.094-74), CDMF, and FAPESP/CEPID (2013/0296-2), for the financial support and to CAPES for the master's scholarship. Dr. A. Leyva (USA) provided English editing of the manuscript.

## REFERENCES

- [1] I.N. Murthy, J.B. Rao, *Procedia Environ. Sci.* **35** (2016) 583.
  - [2] E.B. Ferreira, E.D. Zanotto, L.A.M. Scudeller, *Quim. Nova* **25** (2002) 731.
  - [3] L.A.B. Teixeira, E.A. Vieira, J.A. Tenório, R.A.F. Peixoto, J.R. Oliviera, *Rev. Esc. Minas* **64**, 2 (2011) 169.
  - [4] M.F. Sobral, C.W.A. Nascimento, K.P.V. Cunha, H.A. Ferreira, A.J. Silva, F.B.V. Silva, *Rev. Bras. Eng. Agríc. Ambient.* **15**, 8 (2011) 867.
  - [5] A. Deng, P. Tikalsky, *J. Environ. Eng.* **132** (2006) 586.
  - [6] S.M.A.C. Freitas, L.N. Sousa, P. Diniz, M.E. Martins, P.S. Assis, *Clean. Techn. Environ. Policy* **20** (2018) 1087.
  - [7] S.R. Teixeira, M. Romero, J.M. Rincón, *J. Am. Ceram. Soc.* **93**, 2 (2009) 450.
  - [8] S.R. Teixeira, R.S. Magalhães, A. Arenales, A.E. Souza, M. Romero, J.M. Rincón, *J. Environ. Manage.* **134** (2014) 15.
  - [9] M.V. Folgueiras, M. Tomiyama, T.J.B. Schimitt, in *60° Congr. Bras. Cerâm.* (2016).
  - [10] M. Sridharan, T. Ch. Madhavi, *Mater. Today Proc.*, in press.
  - [11] C. Cardoso, A. Camões, R. Eires, A. Mota, J. Araújo, F. Castro, J. Carvalho, *Resour. Conserv. Recycl.* **138** (2018) 130.
  - [12] N. Quijorna, A. Coz, A. Andres, C. Cheeseman, *Resour. Conserv. Recycl.* **65** (2012) 1.
  - [13] A.S.N.M. Teixeira, R.A.L. Soares, P.R.S. Teixeira, *Cerâm. Ind.* **23** (2018) 36.
  - [14] J. Rossa Jr., K.F. Portella, *Cerâmica* **58**, 348 (2012) 542.
  - [15] M. Rajeswaran, P. Prathap, S. Kannan, S. Naveenkumar, *Mater. Today Proc.* **33** (2020) 214.
  - [16] S. Apithanyasai, N. Supakata, S. Papong, *Heliyon* **6** (2020) e03697.
  - [17] M. Celikbilek, A.E. Ersundu, S. Aydın, in “Advances in crystallization processes”, Y. Mastai (Ed.), *InTech* (2012) 127.
  - [18] H. Savabieh, P. Alizadeh, B. Nayebi, F.J. Clemens, *Ceram. Int.* **45** (2019) 8856.
  - [19] E.D. Zanotto, *Braz. J. Phys.* **22** (1992) 77.
  - [20] L. Lianguang, L. Luo, L. Wang, L. Chenga, X. Xu, Y. Yu, Y. Qin, Y. Wu, *Ceram. Int.* **44** (2018) 21277.
  - [21] V.C.S. Reynoso, K. Yukimitu, T. Nagami, C.L. Carvalho, J.C.S. Moraes, E.B. Araújo, *J. Phys. Chem. Solids* **64** (2003) 27.
  - [22] J. Shia, F. He, J. Xie, X. Liu, H. Yang, *J. Non-Cryst. Solids* **491** (2018) 106.
  - [23] H.E. Kissinger, *J. Res. Natl. Bur. Stand.* **57** (1956) 217.
  - [24] E.G. El-Metwally, A.M. Ismail, E.M. Assim, *J. Non-Cryst. Solids* **496** (2018) 48.
  - [25] A.J. Augis, J.E. Bennett, *J. Therm. Anal. Calorim.* **13** (1978) 283.
  - [26] S. Panyata, S. Eitssayeam, G. Rujjanagul, T. Tunkasiri, K. Pengpat, *Ceram. Int.* **43** (2017) S407.
  - [27] W. Chengyu, T. Ying, *Glass Technol.* **24** (1981) 278.
  - [28] M. Hasanuzzaman, A. Rafferty, M. Sajjia, A.-G. Olabi, in “Reference module in materials science and materials engineering”, Elsevier, Amsterdam (2016) 1.
  - [29] W. Höland, G. Beall, *Glass-ceramic technology*, Am. Ceram. Soc. (2002) 372.
  - [30] M. Romero, M. Kovacoca, J.Ma. Rincón, *J. Mater. Sci.* **43** (2008) 4135.
  - [31] Q.-C. Yu, C.-P. Yan, Y. Deng, Y.-B. Feng, D.-C. Liu, B. Yang, *Trans. Nonferrous Met. Soc. China* **25** (2015) 2279.
  - [32] S.R. Teixeira, M. Romero, J.Ma. Rincón, R.S. Magalhães, A.E. Souza, G.T.A. Santos, R.A. Silva, *Mat. Sci. Eng.* **18** (2011) 112020.
  - [33] S.M. Sidel, E. Idalgo, F.A. Santos, K. Yukimitu, J.C.S. Moraes, *J. Exp. Tech. Instrum.* **1** (2018) 1.
  - [34] H. Savabieh, P. Alisadeh, B. Nayebi, F.J. Clemens, *Ceram. Int.* **45**, 7 (2019) 8856.
  - [35] J. Malek, *Thermochim. Acta* **267** (1995) 61.
- (*Rec. 10/11/2020, Rev. 10/02/2021, 16/03/2021, Ac. 10/04/2021*)